

AS  
SL

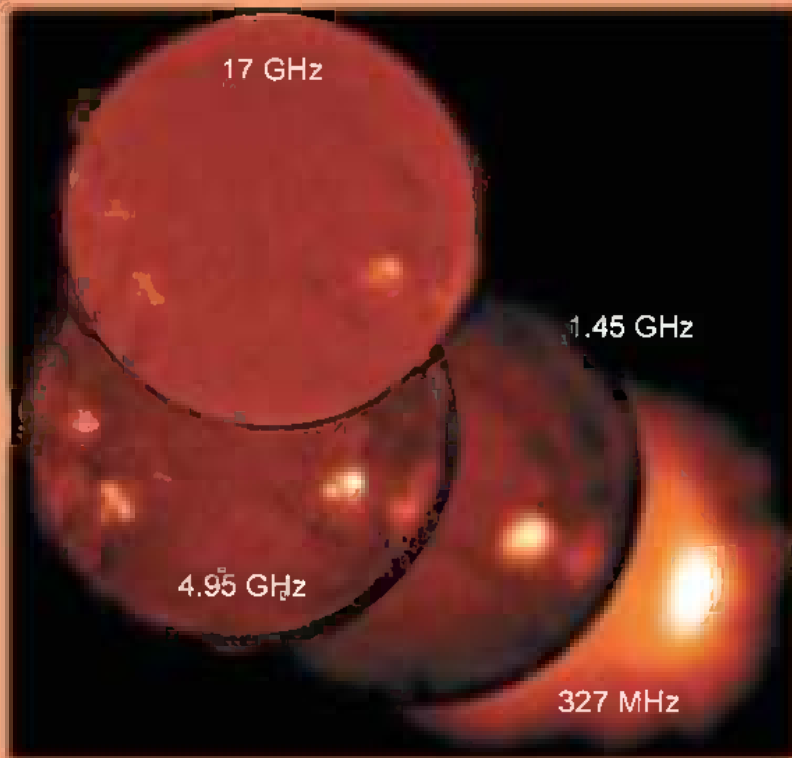
ASTROPHYSICS AND  
SPACE SCIENCE LIBRARY

---

# SOLAR AND SPACE WEATHER RADIOPHYSICS

Current Status and Future Developments

DALE E. GARY  
CHRISTOPH U. KELLER  
Editors



KLUWER ACADEMIC PUBLISHERS

# SOLAR AND SPACE WEATHER RADIOPHYSICS

# ASTROPHYSICS AND SPACE SCIENCE LIBRARY

---

VOLUME 314

---

## EDITORIAL BOARD

### *Chairman*

W.B. BURTON, National Radio Astronomy Observatory, Charlottesville, Virginia, U.S.A.  
(burton@starband.net); University of Leiden, The Netherlands (burton@strw.leidenuniv.nl)

### *Executive Committee*

J. M. E. KUIJPERS, *Faculty of Science, Nijmegen, The Netherlands*  
E. P. J. VAN DEN HEUVEL, *Astronomical Institute, University of Amsterdam,  
The Netherlands*  
H. VAN DER LAAN, *Astronomical Institute, University of Utrecht,  
The Netherlands*

## MEMBERS

I. APPENZELLER, *Landessternwarte Heidelberg-Königstuhl, Germany*  
J. N. BAHCALL, *The Institute for Advanced Study, Princeton, U.S.A.*  
F. BERTOLA, *Università di Padova, Italy*  
J. P. CASSINELLI, *University of Wisconsin, Madison, U.S.A.*  
C. J. CESARSKY, *Centre d'Etudes de Saclay, Gif-sur-Yvette Cedex, France*  
O. ENGVOLD, *Institute of Theoretical Astrophysics, University of Oslo, Norway*  
R. McCRAY, *University of Colorado, JILA, Boulder, U.S.A.*  
P. G. MURDIN, *Institute of Astronomy, Cambridge, U.K.*  
F. PACINI, *Istituto Astronomia Arcetri, Firenze, Italy*  
V. RADHAKRISHNAN, *Raman Research Institute, Bangalore, India*  
K. SATO, *School of Science, The University of Tokyo, Japan*  
F. H. SHU, *University of California, Berkeley, U.S.A.*  
B. V. SOMOV, *Astronomical Institute, Moscow State University, Russia*  
R. A. SUNYAEV, *Space Research Institute, Moscow, Russia*  
Y. TANAKA, *Institute of Space & Astronautical Science, Kanagawa, Japan*  
S. TREMAINE, *CITA, Princeton University, U.S.A.*  
N. O. WEISS, *University of Cambridge, U.K.*

# SOLAR AND SPACE WEATHER RADIOPHYSICS

Current Status and Future Developments

*Edited by*

DALE E. GARY

*Center for Solar-Terrestrial Research,  
New Jersey Institute of Technology, Newark, N.J., U.S.A.*

and

CHRISTOPH U. KELLER

*National Solar Observatory,  
Tucson, AZ, U.S.A.*

**KLUWER ACADEMIC PUBLISHERS**  
NEW YORK, BOSTON, DORDRECHT, LONDON, MOSCOW

eBook ISBN: 1-4020-2814-8  
Print ISBN: 1-4020-2813-X

©2005 Springer Science + Business Media, Inc.

Print ©2004 Kluwer Academic Publishers  
Dordrecht

All rights reserved

No part of this eBook may be reproduced or transmitted in any form or by any means, electronic, mechanical, recording, or otherwise, without written consent from the Publisher

Created in the United States of America

Visit Springer's eBookstore at:  
and the Springer Global Website Online at:

<http://ebooks.springerlink.com>  
<http://www.springeronline.com>

# Contents

List of Figures	xiii
List of Tables	xxi
Preface	xxiii
1	
Solar and Solar Radio Effects on Technologies	1
<i>Louis J. Lanzerotti</i>	
1 Introduction, and Some History	1
2 Electromagnetic Waves and Wireless	2
3 Solar-Terrestrial Effects on Technologies	5
4 Solar Radio Emissions	7
5 Contemporary Solar Radio and Some Implications for Technologies	8
5.1 Solar noise levels and technologies	8
5.2 Solar noise interference	10
5.3 Statistics of solar radio noise	11
6 Conclusion and Looking to the Future	13
References	15
2	
Overview of Solar Radio Physics and Interplanetary Disturbances	17
<i>Monique Pick</i>	
1 General Context of the Radio Emissions	19
2 Coronal Magnetography	20
3 Transient Activity and Flares	24
3.1 Energy dissipation	24
3.2 Solar magnetic reconnection in the solar atmosphere and diagnostics on regions of acceleration	25
3.3 Electron acceleration and transport during flares	28
4 Coronal Mass Ejections	30
4.1 Radio signatures of CMEs	31
4.1.1 Lift-off and angular spread in the corona of flare/CME event	32
4.1.2 Relationship with EUV dimming and coronal waves	34
4.1.3 Direct radio CME imaging	34

5	Coronal and Interplanetary Shocks, Flares and CMES	35
6	Interplanetary Coronal Mass Ejections	37
7	Solar Energetic Particle Events	39
8	Concluding Remarks and the Future of Radio Physics	41
	References	43
3		
	The Frequency Agile Solar Radiotelescope	47
	<i>T. S. Bastian</i>	
1	Introduction and Background	47
2	Preliminaries	49
	2.1 Radiative transfer	49
	2.2 Radio emission mechanisms	50
3	Overview of FASR Science	52
	3.1 Coronal magnetic fields	52
	3.2 The physics of flares	53
	3.3 Drivers of space weather	55
	3.4 The quiet Sun	56
	3.5 Synoptic measurements and forecasting	58
4	Description of the Instrument	59
	4.1 Operational basis	59
	4.2 FASR instrumental requirements	60
	4.3 System design overview	62
	4.3.1 Antenna configuration	63
	4.3.2 Antennas	64
	4.3.3 Feeds and front ends	64
	4.3.4 Signal transmission	65
	4.3.5 Signal processing	66
5	Operational Issues	66
6	Concluding Remarks	67
	References	68
4		
	Radio Spectral Diagnostics	71
	<i>Dale E. Gary, G. J. Hurford</i>	
1	Introduction	71
2	Characteristic Frequencies of the Solar Atmosphere	73
3	Plasma Emission Diagnostics	75
4	Free-Free Diagnostics	75
5	Gyroresonance Diagnostics	77
6	Gyrosynchrotron Diagnostics	81
7	Exotic Mechanisms	83
8	Conclusion	85
	References	86
5		
	Coronal Magnetic Field Measurements through Gyroresonance Emission	89

*Stephen M. White*

1	Coronal Magnetic Fields are Intrinsically 3D	90
2	Extrapolations of Surface Magnetic Fields	91
3	The Properties of Gyroresonance Emission	92
	3.1 Physical mechanism	92
	3.2 Opacity	93
4	Gyroresonance Radio Emission from Active Regions	96
	4.1 Radio emission from a dipole magnetic field	96
	4.2 The effect of viewing angle	98
	4.3 Variation with frequency	98
5	Observational Examples	101
6	Applications of Gyroresonance Emission	104
	6.1 Coronal magnetic field measurement	104
	6.2 Simulations of FASR magnetic field measurements	106
	6.3 Coronal currents	107
	6.4 Tests of magnetic extrapolations	108
	6.5 Heights of radio sources	111
7	Summary	111
	References	112

6

Coronal Magnetic Field Measurements Through Bremsstrahlung 115

*G.B.Gelfreikh*

1	Introduction	115
2	Basic Formulae	115
	2.1 Equations of transfer	115
	2.2 Basic expression for isotropic plasma	117
	2.3 Basic expression for anisotropic plasma	117
3	Diagnostics of the Coronal Plasma	118
	3.1 Diagnostics of the mechanism of the emission generated by thermal bremsstrahlung	118
	3.2 Expressions for the magnetic field	119
	3.3 Radio measurements of the magnetic field	120
4	Expected Parameters of Polarized Radio Emission	121
	4.1 Optically thin regions	121
	4.2 Optically thick regions	122
	4.3 Combination of optically thin and thick regions	123
5	Radio Magnetograms of Solar Active Regions	124
6	Magnetic Fields in Prominences	125
7	Magnetic Fields in a Coronal Hole	127
8	Magnetic Fields in Coronal Loops	130
9	Future Development of the Method	131
	References	133

7

Coronal Magnetic Field Measurements Through QT-Propagation 135

*Boris Ryabov*



1	Microwave QT-Propagation in the Solar Corona	135
1.1	Introduction	135
1.2	Effects of electromagnetic wave mode coupling	137
1.3	Geometry of QT-propagation	140
2	Results and Prospects of Microwave Observations	140
2.1	Regularities of the inversion phenomenon	141
2.2	Multiple inversion	144
2.3	Linear polarization in the outer corona	145
2.4	Oscillations	145
3	The Technique of Coronal Magnetography Through QT-Propagation	147
3.1	Normalization procedure	147
3.2	The source-QTR distance	148
3.3	Scrutiny of a coronal magnetogram	149
4	Summary and Conclusions	150
	References	151
8	Overview of Solar Flares	153
	<i>Hugh Hudson, Lyndsay Fletcher, Josef I. Khan and Takeo Kosugi</i>	
1	Introduction	154
2	New Observational Capabilities	154
2.1	<i>Yohkoh</i>	154
2.2	SOHO and TRACE; other facilities	155
3	The Flare Concept	155
3.1	Confined and LDE flares	156
3.2	Flares and CMEs	156
4	Flare Loops	157
4.1	Footpoints, coronal spectroscopy, and evaporation	158
4.2	Arcades	159
4.2.1	“Sigmoids” and filament cavities	162
4.3	Loop-loop interactions	163
5	Particle Acceleration	163
5.1	Footpoint sources	164
5.2	Coronal sources	164
5.3	Energetic ions	166
6	Ejections	166
6.1	Parallel and perpendicular flows	166
6.2	Dimming	167
6.3	Global waves	168
7	Microflares and Nanoflares	169
8	Evolution of Flare Theories and Models	172
9	Conclusions	172
	References	173
9	Electron Transport During Solar Flares	179
	<i>Jeongwoo Lee</i>	
1	Introduction	179

2	The Formulations	182
2.1	Trap-and-precipitation	182
2.2	Trap, bypass, and precipitation	183
3	Electron Trapping And Precipitation	184
3.1	Simple bursts	184
3.2	Trap or precipitation?	184
3.3	Extended and evolving trap	186
3.4	Trap without precipitation	187
4	Electron Pitch Angle Variation	189
4.1	Weak diffusion	189
4.2	Intermediate diffusion	191
4.3	Strong diffusion	193
4.4	Pitch angle scattering and MWR maps	196
5	Electron Energy Variation	197
6	Concluding Remarks	198
	References	200
10	Decimeter Burst Emission and Particle Acceleration	203
	<i>Arnold O. Benz</i>	
1	Introduction	204
2	The Decimeter Range	204
2.1	Spectral types and classifications	205
2.2	High-frequency limit of the decimeter range	209
2.3	Why decimetric radio bursts?	210
3	Hard X-rays and Decimeter Radiation	211
3.1	Decimetric type III bursts	211
3.2	Decimetric narrowband spikes	211
3.3	Drifting pulsating structures	212
3.4	Flares without radio emission	212
4	Flare Physics	214
4.1	Location of source regions	214
4.2	Evidence for reconnection	215
5	Emission Processes	217
5.1	Beam emissions	217
5.2	Emissions from the acceleration site	218
5.3	Decimetric spikes and pulsations	219
6	Conclusions	219
	References	220
11	Radio Observations of Coronal Mass Ejections	223
	<i>Angelos Vourlidas</i>	
1	Coronal Mass Ejections	223
1.1	A brief CME primer	223
1.2	Radio emissions associated with CMEs	225
1.2.1	Thermal free-free	225
1.2.2	Nonthermal gyrosynchrotron	226

1.2.3	Non-thermal plasma emissions	227
2	Radio CME Observations During Cycle 23	227
2.1	CME detection	229
2.2	CME development	229
2.3	Detection of CME-associated structures	231
2.4	Radio prominence eruptions	232
2.5	Type II emission	233
2.6	CME radio precursors	234
2.7	Overview	234
3	FASR Connection	235
3.1	Advantages of radio observations	235
3.2	Disadvantages of current radio observations	236
3.3	Instrument requirements	236
	References	239
12		
	Tomographic 3D-Modeling of the Solar Corona with FASR	243
	<i>Markus J. Aschwanden, David Alexander, Marc L. DeRosa</i>	
1	Introduction	244
2	Active Region Modeling	245
2.1	Simulation of FASR images	245
2.2	Peak brightness temperature	248
2.3	Temperature and density diagnostic of loops	252
2.4	Radio versus EUV and soft X-ray diagnostics	255
3	Chromospheric and Coronal Modeling	257
4	Future FASR Science	261
	References	262
13		
	Coronal Diagnostics with Radio and EUV/Soft X-Ray Observations	265
	<i>Jeffrey W. Brosius</i>	
1	Introduction	265
2	2D Coronal Magnetography	267
3	Diagnostics of Quasi-Transverse Layers	270
4	Coronal Iron Abundance	271
5	3D Coronal Magnetography	273
6	Future of Coordinated Radio and EUV/Soft X-ray Observations	281
	References	284
14		
	Radio Observations of the Quiet Sun	287
	<i>Christoph U. Keller and Säm Krucker</i>	
1	Introduction	287
2	Observing the quiet Sun at radio wavelengths	289
3	General appearance of the quiet Sun in radio waves	291
3.1	Submillimeter observations	292
3.2	Millimeter and microwave observations	292
4	Thermal stratification of the quiet Sun	294

5	Filaments and prominences	296
6	Coronal heating events in the quiet Sun	297
7	FASR and the quiet Sun	300
	References	301
15		
	Interplanetary Radio Bursts	305
	<i>N. Gopalswamy</i>	
1	Introduction	305
2	Type III Bursts	307
	2.1 Isolated type III bursts	308
	2.2 Complex type III bursts	309
	2.2.1 Origin of nonthermal electrons	310
	2.2.2 Complex type III bursts and CMEs	311
	2.3 Type III storms	312
	2.3.1 Cessation and recovery of type III storms	313
3	Type II Bursts	314
	3.1 IP shocks, CMEs and type II radio bursts	316
	3.1.1 DH type II bursts	317
	3.2 Are type II bursts CME-driven?	318
	3.3 What is a fast CME?	320
4	Recent Developments	323
	4.1 Radio signatures of CME interaction	323
	4.1.1 Radio signature solely due to CME interaction	323
	4.1.2 Medium modification: Interaction between two fast CMEs	324
	4.1.3 Interaction between CMEs with nearly equal speeds	325
	4.1.4 What we mean by CME interaction	325
	4.2 Unusual radio signatures	328
5	Concluding Remarks	329
	References	330
16		
	Solar Radar	335
	<i>William A. Coles</i>	
1	Introduction	335
2	Theory	336
3	Other Coronal Observations	342
4	Previous Radar Measurements	345
5	New Observations	348
6	Use of an Imaging Receiver	351
	References	352
17		
	Three-Dimensional Tomography Of Interplanetary Disturbances	355
	<i>Bernard V. Jackson, P. Paul Hick</i>	
1	Introduction	356
2	Global Data Analyses	358
	2.1 IPS measurements	359

2.2	Helios spacecraft Thomson scattering measurements	362
3	Model and Tomographic Analysis	366
3.1	Solar wind model	367
3.2	Computer analysis	368
4	<i>In-situ</i> Comparisons	371
4.1	Reconstructed global observations	374
5	Conclusion	381
	References	382
	Index	387

# List of Figures

1.1	Signal strengths and sunspot numbers for 1915–1932	4
1.2	Radio strength vs. sunspot numbers for 1926–1928	5
1.3	Timeline for selected major impacts on technical systems	6
1.4	Variation with time of several solar-originating phenomena measured near Earth during the year 1991	9
1.5	Number of solar burst events per day with amplitudes $> 10^3$ SFU	12
1.6	Number of radio events per day vs. peak flux density	14
2.1	The Sun seen at 17 GHz and EUV	18
2.2	Physical maps from microwave imaging spectroscopy	21
2.3	Coronal magnetic field strength at different heights	23
2.4	The frequency distribution of peak rates in hard X rays	26
2.5	Hard X-ray images of an impulsive west limb flare	27
2.6	Spectrogram of metric spikes (above 320 MHz) and type III bursts (below 320 MHz)	28
2.7	Diagram of a flare model envisioning magnetic reconnection and chromospheric evaporation processes	29
2.8	RHESSI observations of the initial rise of an intense solar gamma-ray line flare	30
2.9	Time-lapse images taken by LASCO-C1 coronagraph in Fe XIV emission line.	32
2.10	Solar manifestations associated with CMEs	33
2.11	Example of an EIT wave from 1997 September 24	35
2.12	Type II emission and CME in the 1998 April 20 event	36
2.13	A hectometric interplanetary type II burst in the 1–14 MHz range	38
2.14	Idealized sketch of a complete radio event (from Wild <i>et al.</i> 1963)	40
4.1	Characteristic radio frequencies for the solar atmosphere	74
4.2	A “Universal Spectrum” for free-free brightness temperature	77

4.3	Longitudinal magnetic field from a model atmosphere compared with the field deduced from radio spectra from the model	78
4.4	“Universal Spectra” for gyroresonance emission.	80
4.5	Radio emission spectra at two lines of sight in a model active region, as calculated at 100 frequencies from 1–24 GHz	81
4.6	“Universal Spectra” for gyrosynchrotron emission	83
4.7	Gyrosynchrotron emission from a model coronal magnetic loop	84
5.1	Integrated optical depth of the $s = 2, 3, 4$ gyroresonance layers	95
5.2	Plots of the gyroresonance layers of a dipole sunspot model and the predicted brightness temperatures when the spot is viewed nearly vertically	97
5.3	Same as Figure 5.2, except that now the sunspot is viewed from an angle of $20^\circ$	99
5.4	Brightness-temperature profiles across the dipole sunspot model of Figure 5.2 at various frequencies	100
5.5	Spectra of the brightness temperature at different locations across the spot in Figure 5.4	101
5.6	Brightness-temperature profiles across an isolated sunspot observed with the VLA near disk center	102
5.7	VLA observations of a sunspot at 8.0 GHz	103
5.8	Contours of magnetic field strength at the base of the corona plotted on white light, magnetogram and TRACE images of a sunspot	105
5.9	Two examples of radio spectra from an active region model, showing the technique of determining coronal magnetic field	108
5.10	The results of applying the gyroresonance spectral technique to the entire active region model	109
5.11	VLA observations of a complex solar active region reflecting the magnetic field and temperature distribution in the corona over the active region	110
6.1	Radio maps of an AR observed using the Nobeyama radio heliograph	126
6.2	Radio scan of a prominence at a wavelength $\lambda = 2.1$ cm made with the RATAN-600	127
6.3	One-dimensional radio scans of the sun made with the RATAN-600 at eleven wavelengths in the range 1.8–28 cm	129

6.4	Magnetic field of a coronal hole obtained from observations with the RATAN-600	130
6.5	Radio scans of the Sun at 1.8 cm made with the RATAN-600	131
6.6	Radio emission spectra of a CME-associated coronal loop obtained with the RATAN-600	132
7.1	Comparison of radio maps of circular polarization with a longitudinal magnetogram	138
7.2	Simulated geometry of QT-propagation of microwaves	141
7.3	Circularly polarized microwave sources simulated with due regard to the QT-propagation of microwaves	142
7.4	Radio maps in Stokes $I$ and circular polarization taken with the SSRT at 5.7 GHz	143
7.5	Same region as in Figure 7.4, at 17 GHz one day later	144
7.6	Representative geometry of QT-propagation of microwaves	146
7.7	Details of the inversion phenomenon presented in Figure 7.4	148
7.8	Two coronal magnetograms showing the strength of coronal magnetic fields	149
8.1	Soft and hard X-ray observations of the “Masuda flare”, 1992 January 13, which nicely illustrates the coronal loop structure of a flare	158
8.2	<i>Yohkoh</i> SXT difference image and TRACE image of the arcade flare of 2000 July 14 (“Bastille Day flare”)	160
8.3	A beautiful cusp (following an X-class flare) as observed by SXT	161
8.4	Soft X-ray observations of a spiky arcade event exhibiting the “SAD” phenomenon	162
8.5	Disappearing trans-equatorial interconnecting loop (TIL) associated with a blast wave and CME	168
8.6	Soft X-ray signature of a wave event	170
8.7	Energy distributions for microflares observed with the <i>Yohkoh</i> SXT	171
9.1	Comparison of the radio time profiles for an event at 17 GHz and 34 GHz with a trap model	185
9.2	Lightcurves at microwaves and hard X rays of an impulsive burst	186
9.3	Microwave bursts indicative of long-term trapping	188
9.4	Microwave and hard X ray lightcurves during the Bastille Day flare on 2000 July 14	190
9.5	Microwave maps and spectra obtained for the 1993 June 3 flare	192



9.6	The 1999 August 20 flare as a case of the intermediate pitch angle diffusion	194
9.7	A loop top source near the solar limb observed with NoRH at 34 GHz	195
10.1	Broadband spectrogram recorded with the Phoenix-2 showing a rich event in meter and decimeter wavelengths	206
10.2	Dynamic spectrogram of total flux of an intense type III burst (U shape)	207
10.3	Dynamic spectrogram of total flux showing coherent emission	209
10.4	Dynamic spectrograms of 0.3–4.5 GHz total flux observed with the Phoenix-2 and Ondrejov spectrometers	213
10.5	Location of two clusters of decimetric spikes observed by the Nançay Radioheliograph at 432 MHz	215
10.6	TRACE images overlaid with NRH and Yohkoh/HXT contours of a double-ribbon flare	216
11.1	Halo CME observed by LASCO/C2 and a typical 3-part CME on the west limb	224
11.2	Simulated free-free radio spectra for the quiet Sun and a typical CME	226
11.3	An example of fairly complete spectral coverage of a CME event from 2 GHz to 100 kHz	228
11.4	Radio source progression seen by the NRH at 3 distinct frequencies	230
11.5	Schematic of CME development as inferred from NRH observations.	230
11.6	EIT 195 Å difference image showing the dimming region, overplotted with Nançay 236 MHz contours	231
11.7	Snapshot map of the radio CME loops at 164 MHz	232
11.8	Simulation of CME detection by a temporally redundant array	238
12.1	Potential field extrapolation of SOHO/MDI magnetogram data	246
12.2	Distributions of loop lengths $L$ , loop maximum temperatures $T_{e,max}$ , loop minimum densities $n_{min}$ , and maximum densities $n_{max}$	248
12.3	Simulation of radio brightness temperature maps of an active region at 20 frequencies, from $\nu=100$ to 1258 MHz	249
12.4	Similar representation as in Fig. 12.3, for frequencies of $\nu = 0.8$ to 10 GHz	250

12.5	Radio peak brightness temperature as a function of frequency for the background corona ( $B$ ), for cool ( $C$ ) fat loops, and for hot ( $H$ ) thin loops	251
12.6	Variation of the radio brightness temperature spectrum of a loop with temperature, electron density, and loop width	254
12.7	Enlarged detail of a active region model with a bright loop	256
12.8	Quiet Sun brightness temperature spectrum for an isothermal corona	258
12.9	A compilation of chromospheric and coronal density models	260
12.10	Quiet Sun brightness temperature spectrum for an isothermal corona, for the coronal model by Gabriel (1976), and for a modified Gabriel model	261
13.1	CDS and SERTS spectra from the 1997 November 18 rocket flight	273
13.2	EIT image of NOAA AR 8108 with VLA contours, MDI $B_z$ contours, CDS and SERTS sub-FOV, radio centroids and area for magnetography	274
13.3	$B(T)$ at the centroid of the $R$ component of the 4.866 GHz emission, for four combinations of density distribution	279
13.4	“Slices” of $B(x, y, T)$ along isothermal surfaces	280
13.5	Observed radio maps, with observed and calculated brightness temperature contours	281
13.6	$B(h)$ derived with $n_e$ =constant and different magnetic scale heights	282
13.7	Alfvén speed derived with $n_e$ =constant and $p_e$ =constant	283
14.1	The quiet Sun at different radio wavelengths	291
14.2	Comparison of photospheric magnetogram and 2-cm radio map	293
14.3	Variability of the quiet Sun radio flux at 2 cm	298
14.4	Comparison of network flares in soft X-ray and radio waves at 2 cm	299
15.1	Level of IP radio burst (types II and III) flux compared to cosmic background noise and quiet coronal emission	306
15.2	Hiraiso and Wind/WAVES dynamic spectra showing isolated type III bursts and a type II burst	309
15.3	A complex type III burst that started below about 7 MHz, but was very intense at kilometric wavelengths	310
15.4	Height-time plots of all CMEs that occurred on 2000 November 24, along with the WAVES/RAD2 dynamic spectrum	313

15.5	A hybrid dynamic spectrum consisting of Potsdam and Wind/WAVES data	314
15.6	Type III storm activity observed by Wind/WAVES	315
15.7	IP Type II burst of 2001 September 24-25	316
15.8	Speed, width and acceleration of 132 CMEs associated with DH type II bursts	318
15.9	Histogram of fast CMEs that did not have associated DH type II bursts	319
15.10	Speed distribution of CMEs associated with metric type II bursts as compared to that of general population of CMEs and DH CMEs	320
15.11	Radial profiles of the fast mode speed in the active region and quiet corona	322
15.12	Two CMEs observed by SOHO/LASCO and the associated continuum radio emission detected by Wind/WAVES	324
15.13	SOHO/LASCO difference image showing two interacting CMEs, the associated DH type II bursts, and CME height-time plots	326
15.14	Wind/WAVES dynamic spectrum of the 2001 November 22 events	327
15.15	Wind/WAVES dynamic spectrum of unusual and broadband radio emission that lasted for 4 days	328
15.16	Number of type II bursts that begin in the DH domain and continue to the kilometric domain plotted as a function of time	329
16.1	Plasma density versus solar distance and reflection height versus frequency	337
16.2	Plasma delay and loss versus frequency for the models given in Figure 16.1	338
16.3	Simulation of a spherically symmetric density step of moving outwards at 200 km/s	339
16.4	Simulation of $n_e$ vs radial and tangential distance	341
16.5	Simulation of $n_e$ in the equatorial plane	342
16.6	A relatively simple large CME known as “the lightbulb” as observed by LASCO C2 and C3	343
16.7	Average range distribution of echoes observed with El Campo radar	346
16.8	Annual average radar echo strength	347
16.9	Daily measurements of radar echo strength	347
16.10	Range-Doppler spectra of selected strong echoes	348
16.11	Typical Range-Doppler spectra	349

17.1	Normalized weighting functions for Cambridge and Nagoya interplanetary scintillation (IPS)	361
17.2	Contour plot images obtained from the <i>Helios</i> photometers of the 1979 May 07 CME on May 08 and May 09	364
17.3	Thomson-scattering weight function as a function of distance along the LOS	365
17.4	Schematic of a LOS projected as a reference surface on consecutive days	369
17.5	Time series showing a sample of the final velocity and $g$ -level model compared with observations for a time-dependent tomographic run	371
17.6	Time series showing a sample of the final model and photometer brightness comparison for a time-dependent tomographic run for <i>Helios</i>	372
17.7	10-day velocity time series from the three-dimensional time-dependent model compared to the velocity and density time series from the ACE spacecraft and its correlation	373
17.8	Comparison plot of heliospheric densities at the <i>Helios</i> 2 spacecraft and least squares correlation	374
17.9	View of the corotating component of the plasma density in the inner heliosphere and a three dimensional model projection of the heliosphere	375
17.10	LASCO C2 images and a view of the reconstruction of the halo CMEs	377
17.11	Solwind coronagraph image of the 7 May CME and the remote observer view of heliospheric density	378
17.12	Reconstruction using <i>in-situ</i> observations from 5 spacecraft and using the IPS time-dependent Thomson scattering tomography	378
17.13	Carrington synoptic maps of density and velocity during two halo CMEs	379
17.14	Carrington synoptic map of the heliospheric structure at 1 AU on 1979 May 10	380
17.15	Carrington synoptic map of the heliospheric structure at 0.6 AU on 1977 November 25	381